 doi:10.20944/preprints202201.0278.v1

Construction and Evaluation of Plasmonic Refractive Index Sensor Based on Changing the Number of Resonators and Changing Their Dimensions

Hamid Abbasi
University of Mazandaran, Iran.
abbasiamolihamid6@gmail.com

Abstract: In this paper, a plasmonic refractive index sensor based on MIM waveguide (metal_insulation_metal) with two plasmonic waveguides and five rings and two teeth and four rectangular cavities is proposed and designed. The refractive index of the resonators as well as the resonant wavelengths will be investigated by the time difference finite difference method. To achieve an optical sensor with excellent quality and performance, we change the number and type of amplifiers and their dimensions. In each stage of the simulation, we will only change the refractive index of the middle ring located in the middle of the two waveguides, and the refractive index of the other amplifiers remains the same. This challenge will help to form a more appropriate structure for optical sensors. The sensor built in this simulation has a balanced and suitable function for integrated circuits and helps researchers to better understand the design of plasmonic structures. It also has important applications in medical research, health care, drug manufacturing, security monitoring and environmental protection, internal security of countries and the battlefield.
Keywords: *Photonic, plasmonic, surface plasmon, waveguide, resonator, optic.*

1. Introduction

Optical sensors are powerful tools for diagnosis and analysis and have important applications in medical research, healthcare, drug manufacturing, security monitoring and environmental protection, internal security of countries and the battlefield. Also, due to the specific field distribution of the resonances, optical sensors will be highly sensitive to changes in the refractive index of the environment [1]. Therefore, in scientific research, these sensors are used to measure the refractive index. One of the important points in the analysis of optical sensors is that the sensitivity of optical sensors depends on the material and structure of the sensor. Therefore, to further analyze this issue, let us divide the optical refractive index sensors into six using plasmonic and photonic structures [2]:

a. Metal-based propagating plasmonic eigenwave structur [3-12]
b. Metal -based localized plasmonic eigenmode structures [13-18]
c. Dielectric-based propagating photonic eigenwave structures [19-26]
d. Dielectric-based localized photonic eigenmode structures [27-32]
e. Advanced hybrid structures [33-38]
f. 2D material integrated structures [39-42].

In this paper, the first case, a metal-based plasmonic sensor built on a special plasmon wave, surface plasmon polariton (SPP), will be investigated. SPP is an electromagnetic surface wave that propagates at the metal-dielectric interface [43-47]. Because the wave is at the boundary between the conductor and the external environment (such as air or water), these oscillations are very sensitive to any change in this boundary. Polariton superficial plasmons because of the limitation of classical optical diffraction, they have very strong capabilities, so they are used as energy and information carriers in fully integrated circuits and optical devices. Among the various structures of Polarithon, surface plasmons, Insulation-Insulation-Metal (IMI) structures, and Metal-Insulation-Metal (MIM) structures have been proposed as the two most important structures. Our choice in this article is the structure of MIM. Because this structure has support modes with deep sub-wavelength scales, high bandwidth over a very wide range of frequencies, very high optical confinement, and acceptable propagation lengths [48]. Metal-

Preprints (www.preprints.org) | NOT PEER-REVIEWED | Posted: 19 January 2022 doi:10.20944/preprints202201.0278.v1

insulator-metal (MIM) structuresو such as optical filters [49-52], optical switches [53], demultiplexers [54,55] and sensors [56-59], are widely used. also Plasmonic sensors based on MIM waveguide structures, such as asymmetric nanodisk filter and sensor [60–62], side-coupled cavity sensor [63], notch resonator filter and sensor [64], and circular ring filter and sensor [65,66], are one of the most important optical devices, have attracted tremendous attention, and have been investigated widely in recent years. Therefore, in this article, we will start designing and building a refractive index sensor that consists of arrays of metal-insulated-metal waveguides (MIM) and plasmonic resonators.

2. Drawing the structure of the plasmonic sensor and analyzing its structural model

The structure of our proposed sensor consists of two plasmonic waveguides, five rings, two teeth and four rectangular cavities (Fig.1). The two waveguides have a height of W_1 = 50 nm. The middle ring, which is located between the two waveguides, has an outer radius of R_1 = 125 nm and an inner radius of r_1 = 90 nm. Also, two teeth are connected to the middle ring, which has a length of 40 nm and a height of 20 nm. There are four rings in the upper and lower parts of the waveguides, which have an inner radius of $r_2 = r_3 = r_4 = r_5$ = 91 nm and outer radius $R_2 = R_3 = R_4 = R_5$ = 126 nm, respectively. The two monitors P_{in} and P_{out} are input and output monitors, respectively, which are used to measure the input and output waves. The wave transmission is calculated by the following equation:

$T = P_{out} / P_{in}$ (1)

Also, the simulation substrate is made of silver metal and the waveguides and amplifiers are made of air. To show the optical properties of metals in simulation, we use the greeting model:

$\varepsilon(\omega) = \varepsilon_\infty - \omega_p^2 / \omega^2 + i\Upsilon\omega$ (2)

Here ω_p = 1.37 × 1016 refers to bulk frequency for plasma, ε_∞ =1 gives the medium constant for the infinite frequency, γ = 3.21 × 1013 means damping frequency for electron oscillation, and ω shows incident light angular frequency.

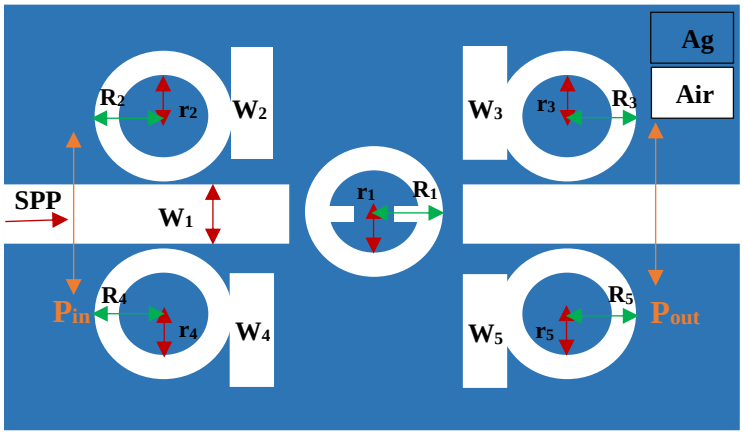

Fig.1. Two-dimensional image of the structure of the designed refractive index sensor.

Because the wavelength of the radiant light is greater than the height of the waveguides, only TM mode can be present in the sensor structure and participate in simulations. The TM wave starts moving from the left and goes through the left waveguide to the resonators. Each resonators reflects or allows a portion of the input wave signal to pass through. Eventually the wave reaches the output waveguide, the intensity of which decreases at the end of the path relative to the beginning of its motion. To explain the electric field distribution, it can be said that energy loss is reduced when the field distribution in structures is equal and similar (Fig. 2). Therefore, in order to achieve the maximum field distribution in the designed sensor structure, all dimensions must be optimal.

Preprints (www.preprints.org) | NOT PEER-REVIEWED | Posted: 19 January 2022 doi:10.20944/preprints202201.0278.v1

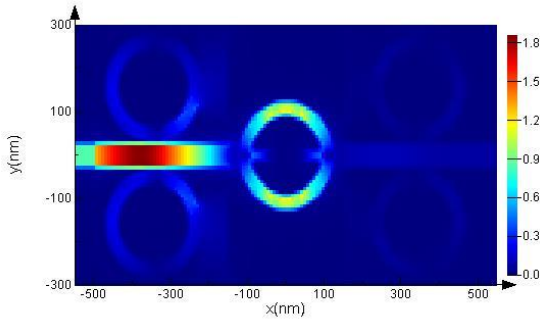

Fig.2. Plasmonic sensor field distribution

3. Sensor design methods using the field-limited difference method and refractive index measurement.

Using the time domain finite difference method, we examine and analyze the sensor performance (numerical analysis) and using the transmission line model method, we theoretically examine the performance of the sensor. Summarizing these two methods, we analyze the proposed structure resonance behavior and get a functional plasmonic sensor. For the numerical approach, we use the finite difference time domain method with exactly the same boundary conditions. Consider the mesh size for both x and y directions, 8 nm. To reduce the simulation time and create a suitable space, we do the simulation in two dimensions. To measure the performance of the sensor and to technically test the designed structure, we examine each of the cavities separately, and in the last step, we examine all the components of the structure as shown in Fig.1. That is, first we analyze this sensor in detail and then in general.

4. Simulation and design of the sensor using two waveguides and a ring with two tooth.

In the first stage, only the middle ring and its two tooth are present, which are placed in the middle of two plasmonic waveguides (Fig.3).

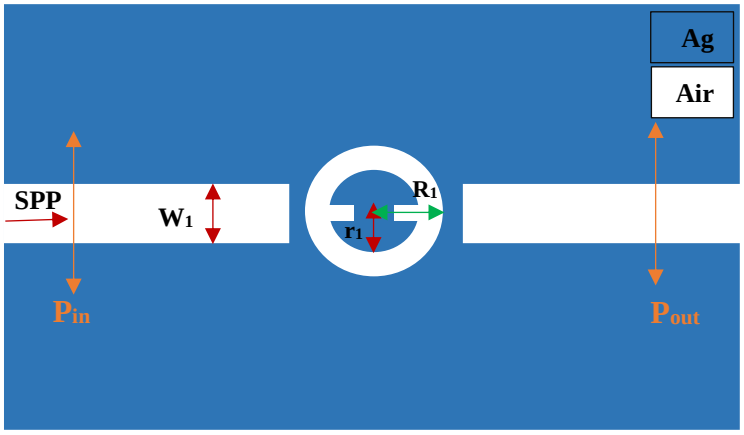

Fig3. Two-dimensional image of the structure of the designed refractive index sensor.

We see the transmission spectrum from the sensor device in Fig.4.

Preprints (www.preprints.org) | NOT PEER-REVIEWED | Posted: 19 January 2022 doi:10.20944/preprints202201.0278.v1

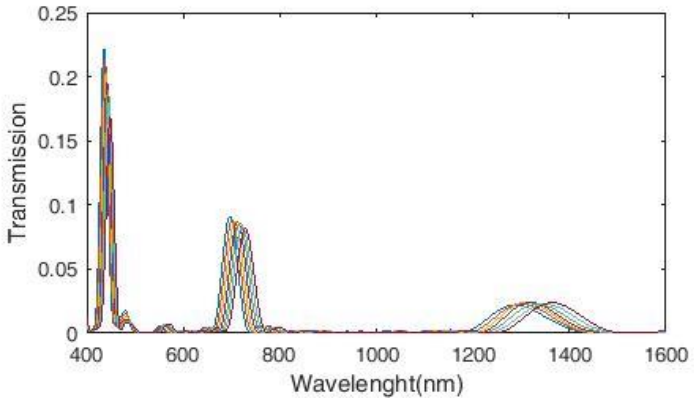

Fig.4. Transmission spectrum of plasmonic refractive index sensor with one ring and two tooth

We change the refractive index of the middle ring with a step of 0.01 nm from 1.14 to 1.2 nm. This will change the resonance spectra and wavelengths. Here we come to the first characteristic of measuring the performance of a sensor, namely S sensitivity:

$S = \Delta\lambda / \Delta n$ (nm / RIU) (3)

In the above equation, Δn is the refractive index change and $\Delta\lambda$ is the resonance wavelength change. By changing the refractive index, the plasmon scattering changes and the resonance point of the structure changes. The graph of the sensitivity coefficient of a plasmonic sensor is shown in Fig.5. According to the figure, the highest sensitivity is related to the refractive index n = 1.2 (in mode 3), which is equal to 1298 nm / RIU.

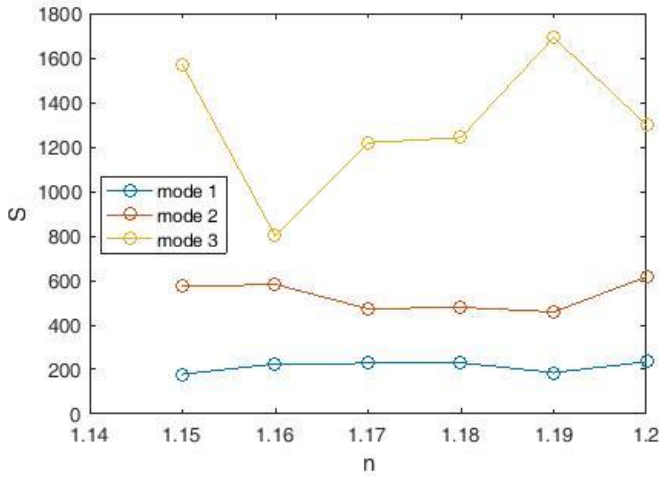

Fig.5. Plasmonic sensor sensitivity coefficient diagram with a ring and two teeth

Next, we calculate and examine the figure of merit (FOM). The obtained diagram (Fig.6) along with the S-sensitivity coefficient diagram will help us to achieve a quality sensor:

FOM = S / FWHM (4)

Preprints (www.preprints.org) | NOT PEER-REVIEWED | Posted: 19 January 2022 doi:10.20944/preprints202201.0278.v1

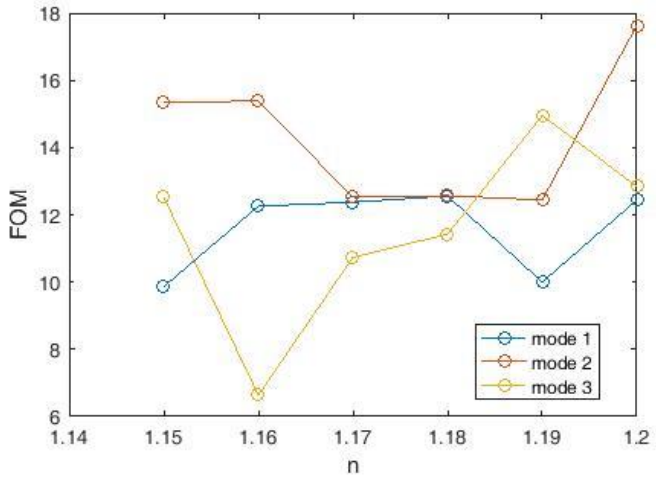

Fig.6. the figure of merit (FOM) Diagram of Plasmonic sensor coefficient.

According to Fig.6, the maximum the figure of merit (FOM) for the refractive index is n = 1.2 (in mode2), which is equal to 17.629 nm / RIU. The last criterion for measuring the designed sensor is Q quality factor:

$Q = \lambda res / FWHM$ (5)

According to Fig.7, the maximum value of the quality factor Q is for the refractive index n = 1.15 (in mode1), which is equal to 24.124 nm / RIU.

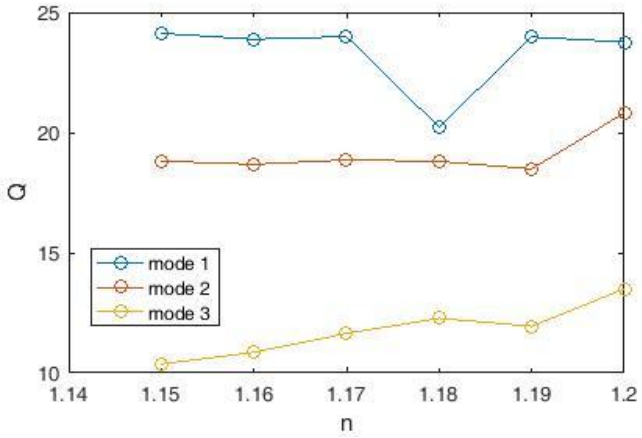

Fig.7. Q-quality coefficient diagram of plasmonic sensor

5. Simulation and design of the sensor using two waveguides and five rings with two tooth

In this step, we seek to improve the performance of the proposed sensor by increasing the number of amplifiers and changing their dimensions and coordinates (Fig.8).

Preprints (www.preprints.org) | NOT PEER-REVIEWED | Posted: 19 January 2022 doi:10.20944/preprints202201.0278.v1

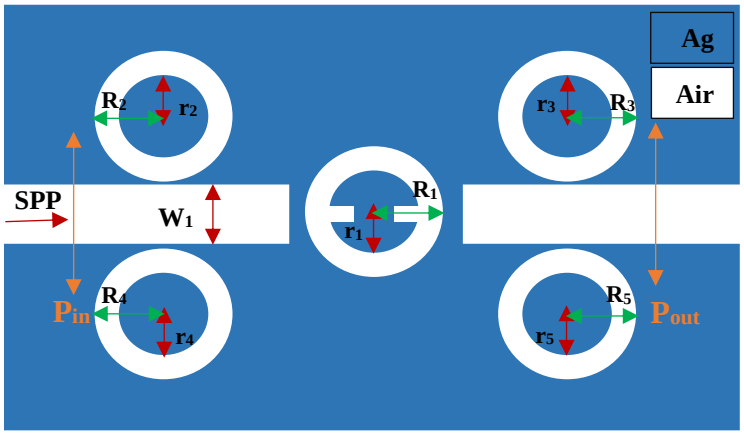

Fig.8. Two-dimensional image of the structure of the designed refractive index sensor.

We see the transmission spectrum of the designed sensor device in Fig.9. This transmission spectrum has three peaks. The left peak has a narrower FWHM and the right peak has a wider FWHM. The middle peak has the highest height. But the right peak will perform better than the other two peaks because it has the highest amount of wavelength change per refractive index change.

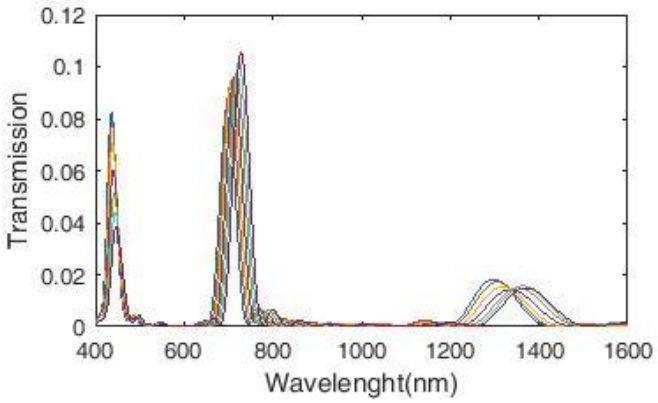

Fig.9. Transmission spectrum of plasmonic refractive index sensor with five rings and two tooth

We will now change the refractive index of the middle ring by 0.01 nm from 1.14 to 1.2 nm and calculate the sensitivity of the proposed sensor. As shown in Fig.10, the highest sensitivity is related to the refractive index n = 1.18 (in mode3), which is equal to 1692 nm / RIU.

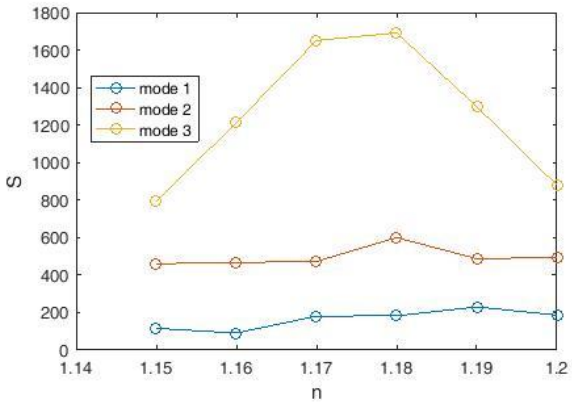

Fig.10. Refractive index sensor sensitivity diagram with five rings and two tooth.

Preprints (www.preprints.org) | NOT PEER-REVIEWED | Posted: 19 January 2022 doi:10.20944/preprints202201.0278.v1

In the continuation of the discussion, we will calculate the figure of merit (FOM) and the quality factor Q and draw the diagrams related to them (Fig.11). According to the figure, the highest figure of merit (FOM) is related to refractive index n = 1.18 (in mode2) which is equal to 14.168 nm / RIU and also, the highest quality factor Q is related to refractive index n = 1.18 (in mode1) Which is equal to 19.994 nm / RIU.

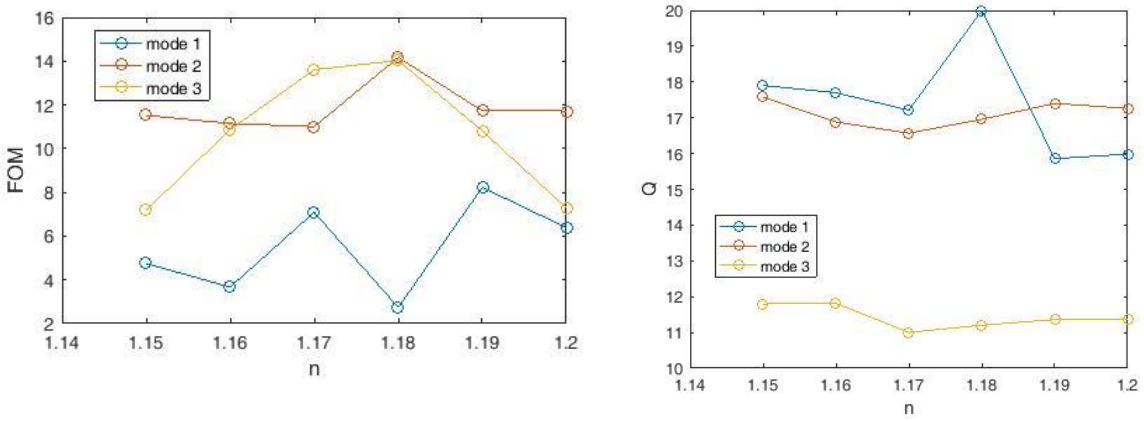

Fig.11. Diagram of figure of merit (FOM) and quality coefficient diagram of Q refractive index sensor with five rings and two tooth.

6 .Simulation and design of the sensor using two waveguides and four cavities and a ring with two tooth

At this stage of the simulation, there are four cavities and a middle ring and two tooth (Fig.12).

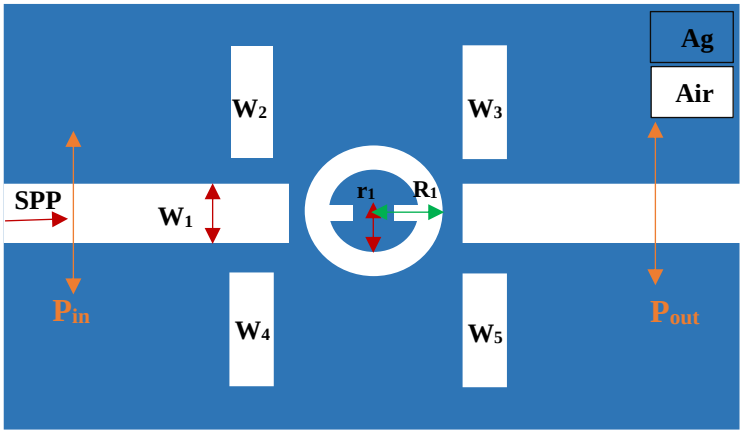

Fig.12. Two-dimensional image of the structure of the designed refractive index sensor.

We see the transmission spectrum of the designed sensor device in Fig.13. The transmission spectrum has three peaks. As in the previous sensor structure (Fig.9), the left peak has a narrower FWHM and the courier on the right has a wider FWHM. But a change has been made compared to the previous structure and the highest height belongs to the left peak. But again, the right peak will perform better than the other two peaks because it has the highest amount of wavelength change per refractive index change.

Preprints (www.preprints.org) | NOT PEER-REVIEWED | Posted: 19 January 2022 doi:10.20944/preprints202201.0278.v1

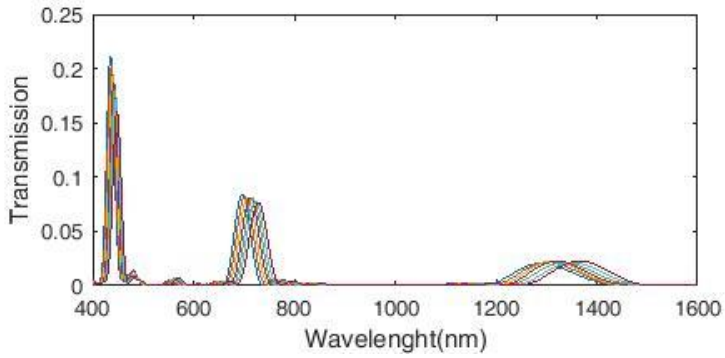

Fig.13. Transmission spectrum of plasmonic refractive index sensor with a ring, two tooth and four cavities

We will now change the refractive index of the middle ring by 0.01 nm from 1.14 to 1.2 nm and calculate the sensitivity of the sensor. As shown in Figure 14, the highest sensitivity is related to the refractive index n = 1.19 (in mode3), which is equal to 1692 nm / RIU.

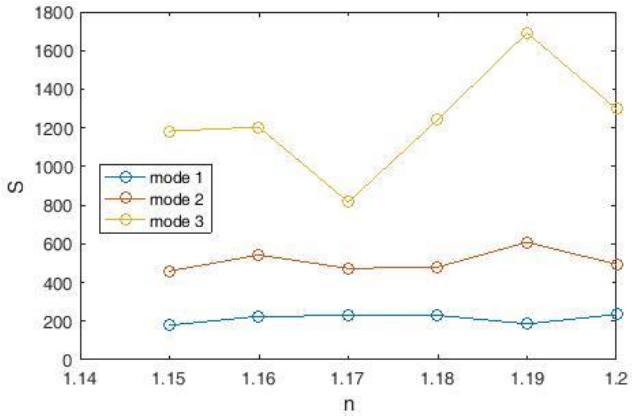

Fig.14. Sensitivity diagram of a refractive index sensor with a ring, two tooth and four cavities.

We will now calculate the values of the figure of merit (FOM) and the quality factor Q and draw diagrams related to them (Fig.15). According to the figure, the highest figure of merit (FOM) is related to the refractive index n = 1.16 (in mode2), which is equal to 14.475 nm / RIU. The value obtained has a higher FOM value than the previous structure (Fig.11). Also, the highest quality factor Q is related to the refractive index n = 1.18 (in mode1), which is equal to 23.99 nm / RIU, which has a higher value of Q than the previous structure (Fig.11).

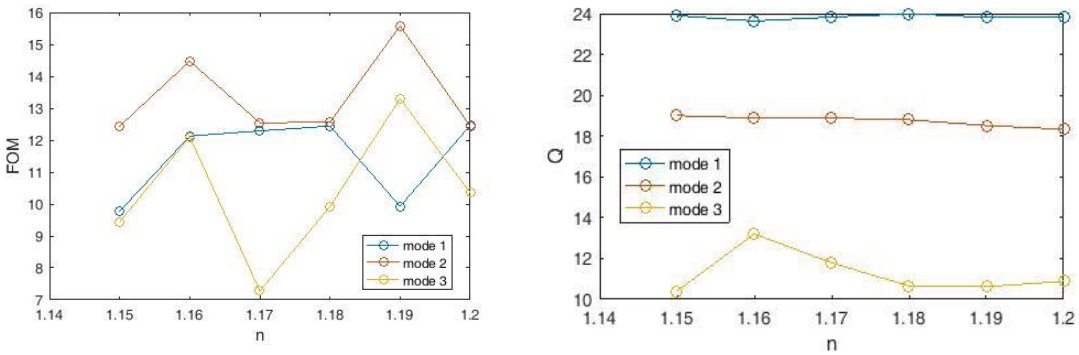

Fig.15. Diagram of figure of merit (FOM) and Q coefficient diagram of sensor with a ring, two tooth and four cavities.

Preprints (www.preprints.org) | NOT PEER-REVIEWED | Posted: 19 January 2022 doi:10.20944/preprints202201.0278.v1

7 .Simulation and design of the sensor using two waveguides and four cavities and five rings with two tooth

In this step of the simulation, we design a plasmonic sensor whose structure is the sum of the two structures of Figures 8 and 12. To use it to reach a general conclusion about the sensor we want. The structure of this sensor will include two waveguides, four cavities and five rings and two tooth (Figure 16).

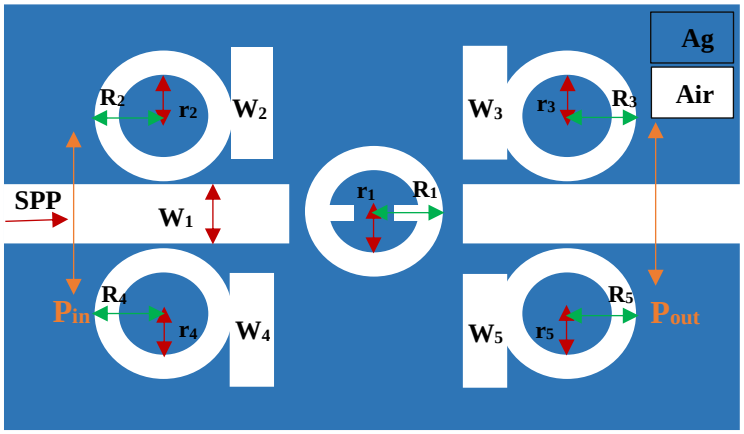

Fig.16. Two-dimensional image of the structure of the designed refractive index sensor.

We see the transmission spectrum of the designed sensor device in Fig.17. This transmission spectrum has two peaks. The courier on the left has a narrower FWHM and the courier on the right has a wider FWHM. The highest height belongs to the peak on the left. But the right peak will perform better than the other peak because it has the highest amount of wavelength change per refractive index change.

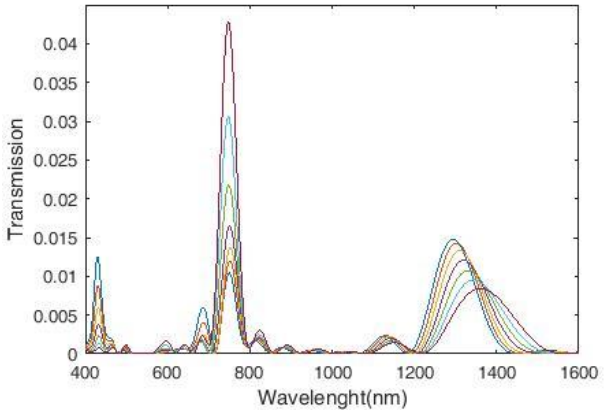

Fig.17. refractive index sensor transmission spectrum with four cavities, five rings and two tooth.

We will now change the refractive index of the middle ring by 0.01 nm from 1.14 to 1.2 nm and calculate the sensitivity of the sensor. According to Fig.18, the highest sensitivity is related to the refractive index n = 1.2 (in mode2), which is equal to 1714 nm / RIU.

Preprints (www.preprints.org) | NOT PEER-REVIEWED | Posted: 19 January 2022 doi:10.20944/preprints202201.0278.v1

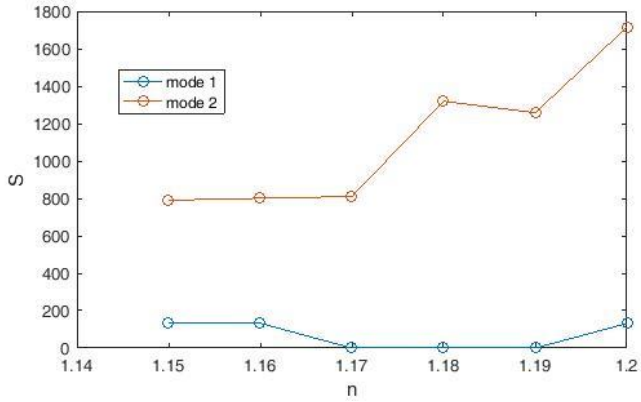

Fig.18. Sensitivity diagram of a refractive index sensor with four cavities, five rings and two tooth.

We will now calculate the values of the figure of merit (FOM) and the quality factor Q and draw diagrams related to them (Fig.19). According to the figure, the highest competence figure (FOM) for the refractive index is n = 1.2 (in mode2), which is equal to 10.407 nm / RIU. Also, the highest quality factor Q is for the refractive index n = 1.15 (in mode1), which is equal to 19.55 nm / RIU.

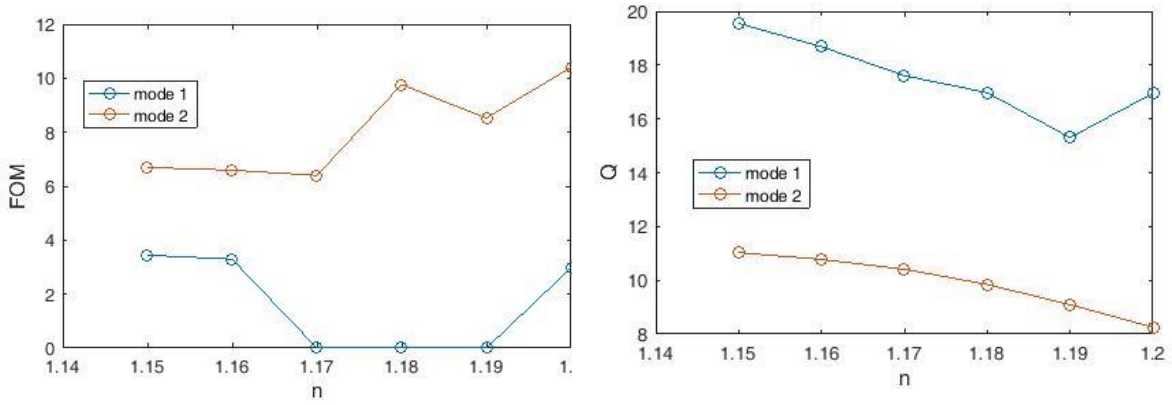

Fig.19. Diagram of figure of merit (FOM) and quality coefficient diagram of Q sensor with four cavities, five rings and two tooth.

8. Conclusion

Refractive index sensors are divided into six categories based on structure (plasmonic and photonic). The dimensions and coordinates of the sensor structure have a great effect on increasing the sensor performance. In this paper, we evaluate sensor performance by changing the coordinates and structure of the sensor and changing the refractive index of the resonators. The resonant wavelength spectrum will change evenly, helping to better design the sensor. Due to its small size and balanced performance, this configuration is suitable for use in integrated circuits.

Reference

[1] Sabine Szunerits, Rabah Boukherroub. Introduction to Plasmonics: *Advancesand Applications*. **2015.**
[2] Optical Refractive Index Sensors with Plasmonic and Photonic Structures: Promising and Inconvenient Truth. Yi Xu,Ping Bai,Xiaodong Zhou,Yuriy Akimov,Ching Eng Png,Lay-Kee Ang,Wolfgang Knoll,Lin Wu, *First published*: 18 February **2019**.
[3] A. Shalabney, I. Abdulhalim, *Opt. Lett*. **2012**, 37, 1175.
[4] J. Dost`alek, H. Vaisocherov`a, J. Homola, Sens. *Actuators*, B **2005**, 108, 758.

[5] S. Nair, C. Escobedo, R. G. Sabat, ACS Sens. **2017**, 2, 379.
[6] Z. Liu, Y. Wei, Y. Zhang, Y. Zhang, E. Zhao, J. Yang, L. Yuan, *Opt. Lett*. **2015**, 40, 2826.
[7] Z. Liu, Y.Wei, Y. Zhang, Y.Wang, E. Zhao, Y. Zhang, J. Yang, C. Liu, L. Yuan, Sens. *Actuators*, B **2016**, 226, 326.
[8] M. D. Baiad, R. Kashyap, *Opt. Lett*. **2015**, 40, 115.
[9] C. Caucheteur, Y. Shevchenko, L. Y. Shao, M. Wuilpart, J. Albert, *Opt. Express* **2011**, 19, 1656.
[10] J.-M. Renoirt, M. Debliquy, J. Albert, A. Ianoul, C. Caucheteur, J. *Phys. Chem.* C **2014**, 118, 11035.
[11] M. Svedendahl, S. Chen, A. Dmitriev, M. Kall, *Nano Lett*. **2009**, 9, 4428.
[12] O. R. Bolduc, L. S. Live, J. F. Masson, *Talanta* **2009**, 77, 1680.
[13] H. Chen, X. Kou, Z. Yang, W. Ni, J. Wang, Langmuir **2008**, 24, 5233.
[14] A. U. Khan, S. Zhao, G. Liu, J. *Phys. Chem*. C **2016**, 120, 19353.
[15] M. R. Gartia, A. Hsiao, A. Pokhriyal, S. Seo, G. Kulsharova, B. T. Cunningham, T. C. Bond, G. L. Liu, Adv. *Opt. Mater*. **2013**, 1, 68.
[16] T. W. Chang, X. Wang, A. Hsiao, Z. Xu, G. Lin, M. R. Gartia, X. Liu, G. L. Liu, Adv. *Opt. Mater*. **2015**, 3, 1397.
[17] Q. Li, X. Zhuo, S. Li, Q. Ruan, Q.-H. Xu, J. Wang, Adv. *Opt. Mater*. **2015**, 3, 801.
[18] K. Lodewijks, W. Van Roy, G. Borghs, L. Lagae, P. Van Dorpe, *Nano Lett***. 2012**, 12, 1655.
[19] Y. Guo, J. Y. Ye, C. Divin, B. Huang, T. P. Thomas, J. R. Baker, Jr, T. B. Norris, Anal. *Chem*. **2010,** 82, 5211.
[20] T. Liu, L. L. Liang, P. Xiao, L. P. Sun, Y. Y. Huang, Y. Ran, L. Jin, B. O. Guan, *Biosens. Bioelectron*. **2018**, 100, 155.
[21] T. Guo, F. Liu, Y. Liu, N. K. Chen, B. O. Guan, J. Albert, *Biosens. Bioelectron*. **2014**, 55, 452.
[22] B. Jiang, K. Zhou, C. Wang, Q. Sun, G. Yin, Z. Tai, K. Wilson, J. Zhao, L. Zhang, *Sens. Actuators*, B **2018**, 254, 1033.
[23] L. Coelho, D. Viegas, J. Santos, J. de Almeida, *Sens. Actuators*, B **2016**, 223, 45.
[24] P. Jia, G. Fang, T. Liang, Y. Hong, Q. Tan, X. Chen, W. Liu, C. Xue, J. Liu, W. Zhang, J. Xiong, *Sens. Actuators*, B **2017**, 244, 226.
[25] A. Farmer, A. C. Friedli, S. M. Wright, W. M. Robertson, *Sens. Actuators*, B **2012**, 173, 79.
[26] A. Sinibaldi, N. Danz, E. Descrovi, P. Munzert, U. Schulz, F. Sonntag, L. Dominici, F. Michelotti, *Sens. Actuators*, B **2012**, 174, 292.
[27] WS Fegadolli, N. Pavarelli, P. O'Brien, S. Njoroge, VR Almeida, A. Scherer, *ACS Photonics* **2015**, 2, 470.
[28] C. Wang, Q. Quan, S. Kita, Y. Li, M. Lonˇcar, Appl. Phys. Lett. 2015, 106, 261105.
[29] G. A. Rodriguez, S. Hu, S. M. Weiss, Opt. Express 2015, 23, 7111.
[30] S. Chandran, R. K. Gupta, B. K. Das, IEEE J. Sel. Top. Quantum Electron. 2017, 23, 8200109.
[31] C. Ca¨er, S. F. Serna-Ot´alvaro, W. Zhang, X. Le Roux, E. Cassan, Opt. Lett. 2014, 39, 5792.
[32] X. Xu, H. Subbaraman, S. Chakravarty, A. Hosseini, J. Covey, Y. Yu, D. Kwong, Y. Zhang, W. C. Lai, Y. Zou, N. Lu, R. T. Chen, ACS Nano 2014, 8, 12265.
[33] Y. Bao, Z. Hu, Z. Li, X. Zhu, Z. Fang, Small 2015,11, 2177.
[34] K. L. Lee, J. B. Huang, J. W. Chang, S. H. Wu, P. K. Wei, Sci. Rep. 2015, 5, 8547.
[35] K. Lodewijks, J. Ryken, W. Van Roy, G. Borghs, L. Lagae, P. Van Dorpe, Plasmonics 2013, 8, 1379.
[36] Y. Wang, L. Wu, TI Wong, M. Bauch, Q. Zhang, J. Zhang, X. Liu, X. Zhou, P. Bai, J. Dostalek, B. Liedberg, Nanoscale 2016, 8 , 8008.
[37] M. D. Baaske, M. R. Foreman, F. Vollmer, Nat. Nanotechnol. 2014, 9, 933.
[38] V. R. Dantham, S. Holler, C. Barbre, D. Keng, V. Kolchenko, S. Arnold, Nano Lett. 2013, 13, 3347.
[39] VG Kravets, R. Jalil, YJ Kim, D. Ansell, DE Aznakayeva, B. Thackray, L. Britnell, BD Belle, F. Withers, IP Radko, Z. Han, SI Bozhevolnyi, KS Novoselov, AK Geim , AN Grigorenko, Sci.
Rep. 2014, 4, 5517.
[40] C. Zhang, Z. Li, S. Z. Jiang, C. H. Li, S. C. Xu, J. Yu, Z. Li, M. H. Wang, A. H. Liu, B. Y. Man, Sens. Actuators, B 2017, 251, 127.
[41] J. C. Reed, H. Zhu, A. Y. Zhu, C. Li, E. Cubukcu, Nano Lett. 2012, 12, 4090.
[42] C. Liu, Q. Cai, B. Xu, W. Zhu, L. Zhang, J. Zhao, X. Chen, Biosens. Bioelectron. 2017, 94, 200.
[43] Barnes, W.L.; Dereux, A.; Ebbesen, T.W. Surface plasmon subwavelength optics. Nature **2003**, 424, 824–830.
[44] Genet, C.; Ebbesen, T.W. Light in tiny holes. Nature **2007**, 445, 39–46.
[45] Neutens, P.; Dorpe, P.V.; Vlaminck, I.D.; Lagae, L.; Borghs, G. Electrical detection of confined gap plasmons in metal-insulator-metal waveguides. Nat. *Photonics* **2009**, 3, 283–286.
[46] Gramotnev, D.K.; Bozhevolnyi, S.I. Plasmonics beyond the diffraction limit. Nat. *Photonics* **2010**, 4, 83–91.
[47]Tunable Plasmonic Band-Pass Filter with Dual Side-Coupled Circular Ring Resonators. Dongdong Liu, Jicheng Wang, Feng Zhang, Yuewu Pan, Jian Lu, and Xiaowu Ni.*Sensors (Basel)*. **2017** Mar; 17(3): 585.

[48] Liu, D.D .; Sun, Y .; Fan, Q.B .; Mei, M.F .; Wang, J.C .; Pan, Y.W .; Lu, J. Tunable plasmonically induced transparency with asymmetric multi rectangle resonators. *Plasmonics* **2016**, 11, 1621–1628.
[49] Lin, X.S.; Huang, X.G. Tooth-shaped plasmonic waveguide filters with nanometeric sizes. *Opt. Lett.* **2008**, 33, 2874–2876.
[50] Lee, T.; Lee, D.; Kwon, S. Dual-function metal-insulator-metal plasmonic optical filter. *IEEE Photonics J.* **2015**, 7, 4800108.
[51] Zand, I.; Bahramipanah, M.; Abrishamian, M.S.; Liu, J.M. Metal insulator-metal nanoscale loop-stub structures. *IEEE Photonics J.* **2012**, 4, 2136–2142.
[52] Lu, H.; Liu, X.M.; Mao, D.; Wang, L.R.; Gong, Y.K. Tunable band-pass plasmonic waveguide filters with nanodisk resonators. *Opt. Express* **2010**, 18, 17922–17927.
[53] Tao, J.; Wang, Q.J.; Huang, X.G. All-optical plasmonic switches based on coupled nano-disk cavity structures containing nonlinear material. *Plasmonics* **2011**, 6, 753–759.
[54] Liu, H.Q .; Gao, Y.X .; Zhu, B.F .; Ren, G.B .; Jian, S.S. A T-shaped high resolution plasmonic demultiplexer based on perturbations of two nanoresonators. *Opt. Commun*. **2015**, 334, 164–169.
[55] Wang, G.X.; Lu, H.; Liu, X.M.; Mao, D.; Duan, L.N. Tunable multi-channel wavelength demultiplexer based on MIM plasmonic nanodisk resonators at telecommunication regime. *Opt. Express* **2011**, 19, 3513–3518.
[56] Wu, T.S .; Liu, Y.M .; Yu, Z.Y .; Peng, Y.W .; Shu, C.G .; Ye, H. The sensing characteristics of plasmonic waveguide with a resonator ring. *Opt. Express* **2014**, 22, 7669–7677.
[57] Lin, Q .; Zhai, X .; Wang, L.L .; Luo, X .; Liu, G.D .; Liu, J.P .; Xia, S.X. A novel design of plasmon-induced absorption sensor. Appl. *Phys. Express* **2016**, 9, 062002.
[58] Qu, S.N .; Song, C .; Xia, X.S .; Liang, X.Y .; Tang, B.J .; Hu, Z.D.; Wang, J.C. Detuned plasmonic Bragg grating sensor based on defect metal-insulator-metal waveguide. *Sensors* **2016**, 16, 784.
[59] Qian, Q.L .; Liang, Y.J .; Liang, Y .; Shao, H.Y .; Zhang, M.L .; Xiao, T.; Wang, J.C. Tunable multiple-step plasmonic Bragg reflectors with graphene-based modulated grating. *Sensors* **2016**, 16, 2039.
[60] Zhan, G.Z.; Liang, R.S.; Liang, H.T.; Luo, J.; Zhao, R.T. Asymmetric band-pass plasmonic nanodisk filter with mode inhibition and spectrally splitting capabilities. *Opt. Express* **2014**, 22, 9912–9919.
[61]Lu, H.; Liu, X.M.; Mao, D. Plasmonic analog of electromagnetically induced transparency in multi-nanoresonator-coupled waveguide systems. *Phys. Rev. A* **2012**, 85, 053803.
[62] Wei, W.; Zhang, X.; Ren, X.M. Plasmonic circular resonators for refractive index sensors and filters. *Nona. Res. Lett.* **2015**, 10, 211.
[63] Xie, Y.Y.; Huang, Y.X.; Zhao, W.L.; Xu, W.H.; He, C. A novel plasmonic sensor based on metal-insulator-metal waveguide with side-coupled hexagonal cavity. *IEEE Photonics J*. **2015**, 7, 4800612.
[64] Bahramipanah, M.; Abrishamian, M.S.; Mirtaheri, S.A.; Liu, J.M. Ultracompact plasmonic loop-stub notch filter and sensor. *Sens. Actuators B* **2014**, 194, 311–318.
[65] Zou, S.W.; Wang, F.Q.; Liang, R.S.; Xiao, L.P.; Hu, M. A nanoscale refractive index sensor based on asymmetric plasmonic waveguide with a resonator ring: A review. *IEEE Sens. J.* **2015**, 15, 646–650.
[66] Zhang, H.Y.; Shen, D.L.; Zhang, Y.P. Circular split-ring core resonators used in nanoscale metal-insulator-metal band-stop filters. *Laser Phys. Lett*. **2014**, 11, 115902.